JOURNAL OF PROPULSION AND POWER
Vol. 9, No. 3, May–June 1993

Using a Full Potential Solver for Propulsion System Exhaust Simulation

Robin G. Melvin,* Forrester T. Johnson,† David P. Young,‡ David W. Foutch,§ John E. Bussoletti,¶ and Michael B. Bieterman**
The Boeing Company, Seattle, Washington 98124

The need for accurate simulations of engine installations on modern commercial transport aircraft has led to consideration of several formulations capable of modeling engine exhausts. Since such exhausts often interact with wings, struts, and nacelles, a complex geometry computational fluid dynamics (CFD) capability is desirable. Engine exhausts often contain nonlinear effects such as weak shock waves. There are very few CFD codes that can model these effects for complex geometries in a timely way. However, a full potential formulation has been implemented in the general geometry code TRANAIR. This model incorporates certain assumptions, the main one being that the flowfield can be divided into a finite number of regions in each of which the total pressure and total temperature are constant. The purposes of this article are to state the theoretical assumptions made by the full potential and Euler models and to validate the methods on an axisymmetric test case. In the situations considered (typical of modern turbofan engines) the full potential and Euler results agree very well.

Nomenclature

c = speed of sound
$\boldsymbol{E}$ = energy flux vector
G = swirl
H = enthalpy
M = Mach number
$\mathcal{M}$ = momentum flux tensor
P_T, P_S = total pressure, static pressure
p = pressure
q = velocity magnitude
$\mathcal{R}$ = difference of specific heats
r_P = ratio of local total pressure to total pressure at infinity
r_T = ratio of local total temperature to total temperature at infinity
S = entropy
T = temperature
$\boldsymbol{V}$ = velocity
$\boldsymbol{W}$ = mass flux
α = average quantity
γ = ratio of specific heats
Δ = jump in quantity
μ = doublet parameter
ν_1, ν_2 = upwinding switches
ρ = density
Φ, ϕ = total potential, perturbation potential
$\boldsymbol{\omega}$ = vorticity

Subscripts
r = reference
∞ = freestream

Superscripts
L = lower surface variables
U = upper surface variables
$*$ = substitute flow variables, scaled flow variables

Received April 8, 1992; revision received Nov. 16, 1992; accepted for publication Dec. 31, 1992.

*Senior Principal Scientist, Applied Mathematics and Statistics, Boeing Computer Services, M/S: 7H-96, P.O. Box 3707. Member AIAA.

†Boeing Technical Fellow, Aerodynamics Research, Boeing Commercial Airplane Group, M/S: 7H-96, P.O. Box 3707. Associate Fellow AIAA.

‡Boeing Associate Technical Fellow, Applied Mathematics and Statistics, Boeing Computer Services, M/S: 7H-96, P.O. Box 3707. Member AIAA.

§Aerospace Engineer, Propulsion Research, Boeing Commercial Airplane Group, M/S: 7H-96, P.O. Box 3707.

¶Aerospace Engineer, Aerodynamics Research, Boeing Commercial Airplane Group, M/S: 7H-96, P.O. Box 3707.

**Senior Principal Scientist, Applied Mathematics and Statistics, Boeing Computer Services, M/S: 7H-96, P.O. Box 3707.

I. Introduction

INTEGRATION of propulsion systems is playing an increasingly important role in designing modern aircraft. When commercial jet aircraft were first developed, the engines were placed a significant distance from the wing (e.g., the Boeing 707 or the B-52) so as to minimize "interference drag." Such placement, however, imposes structural penalties, such as the need for longer landing gear and heavier struts. Close integration places severe demands on computational fluid dynamics tools. In addition to the necessity of modeling the entire airframe as a unit, there are also interactions between the engine exhaust and the rest of the airplane. Also, the geometric and physical complexities of the problem require the solution of large computational problems with many degrees of freedom (DOF). In particular, engine exhausts tend to have large areas of supersonic flow, and complex but relatively weak expansion and compression waves and shocks requiring high grid resolution.

The flowfield in fan jet plumes can be modeled by the full, time-dependent Navier-Stokes equations. The difficulties involved in solving these equations are enormous and the Reynolds-averaged Navier-Stokes equations must be used instead. The solution to these equations involves the construction of adequate grids and the development of accurate turbulence models. At high Reynolds numbers viscous effects are confined to boundary layers on solid surfaces and shear layers bounding the plumes. At flight Reynolds numbers it may be possible to ignore even these viscous effects and solve the steady-state Euler equations. For many external-flow problems the full potential approximation to the Euler equations offers reasonable accuracy at considerably reduced expense. However, it is generally thought that the full potential equation does not govern plume flows when there are powered effects. The analysis contained in this article and the results presented in Sec. VI show that this is not necessarily true.

In any modeling situation, general geometry capability must be balanced against the fidelity of the flow physics modeling. The full potential equation was chosen for the TRANAIR code[1,2] because it models important nonlinear effects and is well enough understood to allow development of a reliable general geometry engineering tool. Also, there is only one unknown per grid point, leading to lower storage and CPU time than that required for solution of the Euler or Navier-Stokes equations. On the other hand, there are limits to the type of flowfields that can be modeled by the full potential equation. The Euler equations, having five unknowns per grid point in three dimensions (four per grid point in two dimensions), can model volume vorticity and entropy variations. This results in improvements in accuracy when the flow contains strong shock waves or slip surfaces. The purpose of this article is to try to explain in detail some of these tradeoffs and to compare results from two codes. In order to facilitate the use of extremely fine computational grids, the comparison was made using two-dimensional axisymmetric versions of the TRANAIR code,[1] and the Euler code PARC.[3]

Section II describes the theoretical basis for the application of full potential modeling to powered plumes. Section III briefly describes the TRANAIR full potential code (which has been extended to model powered plumes). Section IV discusses the PARC Euler code used for code comparison. Section V describes the test problem and Sec. VI gives the computational results.

II. Theory Behind Potential Flow Plume Modeling

The analysis contained in this section gives the theory justifying the application of the full potential formulation to the computation of turbofan jet plumes. In Sec. II.D. the main concept which allows the application of standard full potential solvers to a large class of propulsion problems is defined.

A. Euler Equations

The steady-state Euler equations in three dimensions are five equations in five unknowns. These unknowns can be taken to be p, ρ, and the three components of the velocity vector $\boldsymbol{V}$. The Euler equations express conservation of mass, momentum, and energy as follows:

$$\nabla\cdot\boldsymbol{W} = 0, \qquad \boldsymbol{W} = \rho\boldsymbol{V} \tag{1}$$

$$\nabla\cdot\mathcal{M} = 0, \qquad \mathcal{M} = \boldsymbol{W}\boldsymbol{V}^T + pI \tag{2}$$

$$\nabla\cdot\boldsymbol{E} = 0, \qquad \boldsymbol{E} = H\boldsymbol{W} \tag{3}$$

To complete the description, total enthalpy H is defined for an ideal gas

$$H \equiv \{\gamma p/[(\gamma - 1)\rho]\} + \tfrac{1}{2}q^2 \tag{4}$$

where $q = \|V\|_2$. The thermodynamic entropy S can be defined for an ideal gas as follows:

$$(p/p_\infty) = (\rho/\rho_\infty)^\gamma \exp[(\gamma - 1)(S - S_\infty)/\mathcal{R}] \tag{5}$$

Here $\mathcal{R}$ is the difference of the specific heat capacities. By solving Equations (4) and (5) for p and ρ in terms of H, S, and q, the Euler equations can be alternatively cast as five equations for the five variables H, S and $\boldsymbol{V}$. To better understand the Euler equations in terms of these variables, Eqs. (1–3) can be combined in the following ways:

$$(\nabla\cdot\boldsymbol{E}) - H(\nabla\cdot\boldsymbol{W}) \equiv \boldsymbol{W}\cdot\nabla H = 0 \tag{6}$$

$$(q^2 - H)(\nabla\cdot\boldsymbol{W}) - \boldsymbol{V}\cdot(\nabla\cdot\mathcal{M}) + (\nabla\cdot\boldsymbol{E}) \equiv T\boldsymbol{W}\cdot\nabla S = 0 \tag{7}$$

$$(\nabla\cdot\mathcal{M}) - (\nabla\cdot\boldsymbol{W})\boldsymbol{V} \equiv -\boldsymbol{W}\otimes\boldsymbol{\omega} - \rho T\nabla S + \rho\nabla H = 0 \tag{8}$$

Here $\boldsymbol{\omega} = \nabla\otimes\boldsymbol{V}$ is the vorticity vector and $T = p/(\mathcal{R}\rho)$ is the temperature. Equation (8) can be rewritten in an alternative way by introducing the concept of swirl, i.e.

$$G \equiv (\boldsymbol{W}\cdot\boldsymbol{\omega}/\rho^2 q^2) \equiv \text{swirl} \tag{9}$$

Then Eq. (8) becomes

$$\boldsymbol{\omega} = G\boldsymbol{W} + (T/\rho q^2)\boldsymbol{W}\otimes\nabla S - (1/\rho q^2)\boldsymbol{W}\otimes\nabla H \tag{10}$$

Using Eq. (1) and the fact that $\nabla\cdot\boldsymbol{\omega} = 0$, an equation for G is obtained by taking the divergence of Eq. (10), i.e.

$$\boldsymbol{W}\cdot\nabla G = \nabla\cdot[(1/\rho q^2)\boldsymbol{W}\otimes\nabla H - (T/\rho q^2)\boldsymbol{W}\otimes\nabla S] \tag{11}$$

A heuristic idea of how the Euler equations work can be given in such a way that the approximations underlying the use of the full potential equation will be made clear. Given an initial estimate of $\boldsymbol{V}$, an approximate solution to the Euler equations can be obtained by noting that Eq. (6) is a convection equation for H and states that H is constant along streamlines. If H is specified at the head of every streamline, then H may be found at every point in the flowfield. (Possible discontinuities of H, S, and $\boldsymbol{V}$ in the flowfield will be addressed later.) From Eq. (7) it is seen that once S is specified at the head of every streamline it can likewise be convected unchanged along streamlines. Assuming G is specified at the head of every streamline, old estimates of $\boldsymbol{V}$ and new estimates of p, ρ, and T can be used to convect G along streamlines by means of Eq. (11). The vorticity vector $\boldsymbol{\omega}$ can then be computed from Eq. (10). At this point a new estimate of $\boldsymbol{V}$ can be obtained as follows. $\boldsymbol{V}$ is decomposed into the sum of a scalar potential Φ and a vector potential $\boldsymbol{A}$:

$$\boldsymbol{V} = \nabla\Phi + \nabla\otimes\boldsymbol{A}, \qquad \nabla\cdot\boldsymbol{A} \equiv 0 \tag{12}$$

Taking the curl of Eq. (12) gives

$$\nabla^2\boldsymbol{A} = -\boldsymbol{\omega} \tag{13}$$

$\boldsymbol{A}$ can now be computed using standard integral formulas. The only remaining unknown is Φ. Equation (1) can be considered as a second-order equation defining Φ. It can be solved by a full potential flow solver which can handle field sources, using boundary conditions appropriate for potential flow.

Now consider boundary conditions on configuration surfaces. For an impermeable surface the only boundary condition required is

$$\hat{\boldsymbol{n}}\cdot\boldsymbol{V} = 0 \tag{14}$$

For a permeable surface there are two cases depending on whether the streamlines enter or exit the surface. Assume they exit the surface. If the local flow is supersonic then it is known immediately that H, S, and $\boldsymbol{V}$ must all be specified. If the local flow is subsonic, then H, S, and G must be specified together with one additional boundary condition. This condition should be compatible with a well-posed Neumann or Dirichlet condition for Φ. (Note, that there are many equivalent formulations of these boundary conditions. This particular choice is motivated by consideration of the potential flow approximation in Sec. II.C.) Now assume the streamlines enter the surface. If the local flow is supersonic it is known immediately that no conditions may be specified. If the local flow is subsonic then only one boundary condition may be specified, which again must be compatible with a well-posed boundary condition for Φ.

At surfaces of discontinuity in the flowfield (e.g., lateral plume boundaries or shocks) the appropriate jump conditions can be derived by viewing Eqs. (1–3) as flux conservation laws. Denoting by Δ the jump in a quantity across a surface

with normal $\hat{n}$, and by α the average value of the quantity on both sides of the surface, these conservation laws imply

Mass

$$\Delta(\hat{n}\cdot W) = 0 \tag{15}$$

Momentum

$$\Delta(\hat{n}\cdot W)\alpha(V) + \alpha(\hat{n}\cdot W)\Delta(V) + \Delta(p)\hat{n} = 0 \tag{16}$$

Energy

$$\Delta(\hat{n}\cdot W)\alpha(H) + \alpha(\hat{n}\cdot W)\Delta(H) = 0 \tag{17}$$

Substituting Eq. (15) into Eqs. (16) and (17), and splitting Eq. (16) into tangential and normal components, gives

Normal Momentum

$$\alpha(\hat{n}\cdot W)\Delta(\hat{n}\cdot V) + \Delta(p) = 0 \tag{18}$$

Tangential Momentum

$$\alpha(\hat{n}\cdot W)\Delta(\hat{n}\otimes V) = 0 \tag{19}$$

Energy

$$\alpha(\hat{n}\cdot W)\Delta(H) = 0 \tag{20}$$

There are two possibilities depending on whether or not $\alpha(\hat{n}\cdot W)$ is zero.

If $\alpha(\hat{n}\cdot W)$ is not zero, then the discontinuity surface is a shock surface. Conservation of mass [Eq. (15)] shows that $\hat{n}\cdot W$ is continuous across a shock. Conservation of energy in the form of Eq. (20) shows that H is continuous across a shock. Conservation of tangential momentum [Eq. (19)] shows that the tangential components of velocity are continuous across a shock. Conservation of normal momentum [Eq. (18)] combined with conservation of mass [Eq. (15)] yields the Rankine-Hugoniot relations governing the jumps in S and $\hat{n}\cdot V$ across a shock.

If $\alpha(\hat{n}\cdot W) = 0$, then the surface is a slip surface or inviscid wake. Wakes form the lateral boundaries of plumes. From Eqs. (15), (18), (19), and (20), it is seen that the following three conditions are equivalent to conservation of mass, momentum, and energy across wakes:

$$\alpha(\hat{n}\cdot W) = 0 \tag{21}$$

$$\Delta(\hat{n}\cdot W) = 0 \tag{22}$$

$$\Delta(p) = 0 \tag{23}$$

Equations (21) and (22) show that slip surfaces are stream surfaces. Note that entropy, total enthalpy, density, and all three components of velocity may jump across a wake.

B. Role of Total Temperature in the Inviscid Analysis of Plume Flows

It turns out to be somewhat more useful to replace H and S by the more directly measurable, but equivalent parameters r_T and r_P. The parameter r_T is the ratio of the local total temperature to the total temperature at infinity, and is related to H by the formula

$$r_T = \frac{(\gamma - 1)H}{c_\infty^2\{1 + [(\gamma - 1)/2]M_\infty^2\}} = \frac{H}{H_\infty} \tag{24}$$

Here c denotes speed of sound and M denotes Mach number, i.e.

$$c^2 = \gamma p/\rho \qquad M = q/c \tag{25}$$

r_P is related to S and H by the formula

$$r_P = (r_T R)^{\gamma/(\gamma-1)} = \frac{P_T}{p_\infty}\left[1 + \frac{\gamma - 1}{2}M_\infty^2\right]^{[(-\gamma)/(\gamma-1)]} \tag{26}$$

where

$$R = \exp[-(\gamma - 1)(S - S_\infty)/\gamma\mathcal{R}] \tag{27}$$

p_∞ is the static pressure at infinity, and the ratio P_T/p_∞ is the fan or core pressure ratio commonly used in engine performance measurements.

Pressure and density may be expressed as functions of r_T, r_P, and q by the formulas

$$p = p_\infty r_P F^{\gamma/(\gamma-1)} \tag{28}$$

$$\rho = \rho_\infty(r_P/r_T)F^{1/(\gamma-1)} \tag{29}$$

$$F = 1 + [(\gamma - 1)/2]M_\infty^2[1 - (q^2/r_T q_\infty^2)] \tag{30}$$

An important fact concerning inviscid plume flows is that r_T (and equivalently H) is often an unessential variable. Here unessential means that the streamline pattern, Mach number, pressure and momentum (and hence forces) are totally independent of values of H specified at the head of each streamline. To see this, pose and solve a general boundary value problem for the Euler Eqs. (1), (2), and (3). A substitute flow is then defined[4] with new variables p^*, ρ^*, and V^* as follows:

$$V^* \equiv \sqrt{(H_\infty/H)}V$$
$$\rho^* \equiv (H/H_\infty)\rho \tag{31}$$
$$p^* \equiv p$$

It is easy to show that this substitute flow also satisfies the Euler equations in a conservative manner,[5] and moreover, that

$$H^* = \{\gamma p^*/[(\gamma - 1)\rho^*]\} + \tfrac{1}{2}q^{*2} \equiv H_\infty \tag{32}$$
$$M^* = (q^*/c^*) = M$$

where

$$c^{*2} = (\gamma p^*/\rho^*) \tag{33}$$

The existence of such a substitute flow implies that it is always possible to solve the full Euler equations by first solving the mass and momentum equations (four equations in four unknowns) and then performing a postprocessing computation to solve the energy equation. First set $H^* \equiv H_\infty$, define ρ^* by

$$\rho^* \equiv \gamma p^*/[(\gamma - 1)(H_\infty - \tfrac{1}{2}q^{*2})] \tag{34}$$

and solve Eqs. (1) and (2) for V^* and p^*. For this purpose Eqs. (31) and (34) are used to transform the original boundary conditions to boundary conditions for p^* and V^*. Upon solution, H is defined at the head of every streamline as originally specified and its value is convected unchanged down every streamline (even through shocks). Then V, ρ, and p are solved for by inverting Eqs. (31). This completes the procedure. Now, assume the above boundary conditions for V^* and p^* on the configuration surface turn out to be independent of H. (For example, this will be the case for impermeable surfaces, for exits on which the swirl and tangential components of velocity are specified as zero, and for inlets open to the freestream flow.) Then the solution V^*, ρ^*, and p^* is entirely independent of H. By inspection of Eqs. (31–33),

the streamline patterns, pressure and momentum (hence forces), and Mach number are seen to be the same for V, ρ, and p as for V^*, ρ^*, and p^*.

This shows that the solution is essentially independent of the specified values of H (or r_T), and that the only real result of specifying nonfreestream total temperature is to scale the velocity and mass flux vectors.

C. Potential Flow Approximation

Assume H equals a single constant at the head of all streamlines in a stream tube. Then H will be identically constant in the tube and the flow will be isoenergetic. Similarly, assume that S equals a single constant at the head of all streamlines in the tube. In the absence of shocks S will be constant in the tube and the flow will be isentropic. Because S always jumps across shocks, a flowfield which is initially isentropic will not remain so downstream. For weak shocks the entropy jump is quite small and the flow may still be considered isentropic.

If the flow in a tube can be considered isoenergetic and isentropic, then the right side of Eq. (11) vanishes and G is convected unchanged along streamlines in the absence of shocks. Assume that G is zero at the head of every streamline in the tube. Then the flow will initially be swirl-free. G does jump across shocks, but the jump is small for weak shocks and actually zero for normal shocks. Assuming the flow in a tube is isoenergetic and can be considered isentropic and swirl-free, Eq. (10) shows that the vorticity vector vanishes. The velocity vector can then be expressed as the gradient of a scalar potential.

To summarize, the flow in a plume can be considered to be potential flow if 1) variations in entropy and total enthalpy at the exit of the propulsion device are small, 2) the propulsion device produces a negligible amount of swirl, and 3) shocks in the plume are weak.

Assuming the velocity field in a plume can be represented by a potential, set

$$V = \nabla\Phi \tag{35}$$

From Eqs. (28) and (29), p and ρ can be solved for as functions of r_T, r_P, and q. Since r_T and r_P are specified constants in the plume, the only real unknown is Φ and any one of Eqs. (1–3) can be used as the governing flow equation. [Usually, Eq. (1) is chosen.]

At a solid surface with normal vector $\hat{n}$ the condition

$$\hat{n}\cdot W = 0 \tag{36}$$

is required. This is the natural Neumann boundary condition associated with Eq. (1). At the exit of a propulsion device (upstream boundary of a plume), specification of normal mass flux is not well-posed when the Mach number at the exit is subsonic. The amount of mass flow in the plume is actually determined by the Kutta condition at the cowl trailing edge when the flow is not choked, and is therefore dependent on the interaction between the plume and its exterior. Thus, the exit boundary condition must involve primarily the tangential components of velocity. In potential flow the tangential components must be derivable as the surface gradient of a scalar potential. It is the usual practice to specify the actual value of this potential rather than compatible tangential velocity components. Otherwise, the level of potential in the plume would be arbitrary, and therefore, the boundary value problem would be singular. If no other information is available, the potential can be chosen to be constant, which means that the exit flow direction must be normal to the exit surface. The actual value of the constant is immaterial. If the exit Mach number is supersonic, its value must be specified. This is an additional boundary condition which can be implemented in a potential flow solver by upwinding the density at the exit to its value at the specified Mach number.

Across shock surfaces, $\hat{n}\cdot W$ and H are assumed continuous as in Euler flow. Thus, mass and energy are conserved. Conservation of tangential momentum is enforced by requiring the potential itself to be continuous across a shock surface. This condition is equivalent to the continuity of the tangential components of velocity. To maintain potential flow, conservation of normal momentum [Eq. (18)] is replaced by

$$\Delta S = 0 \tag{37}$$

This leads to a modification in the Rankine-Hugoniot relations, which is slight for weak shocks. Most potential flow solvers capture shocks so that these relations are imposed without the necessity of modeling shocks as boundary surfaces.

Full Euler solvers capture wakes in such a manner that Eqs. (21–23) are automatically satisfied, although numerical diffusion tends to smear the slip surfaces. In potential flow, wakes must be modeled as boundary surfaces with jump boundary conditions. Since the full potential equation is a second-order partial differential equation, only two (or two linear combinations) of the three Eqs. (21–23) may be imposed. The remaining condition must be achieved by moving the wake. This topic will be discussed in the next section.

D. Wake Boundary Conditions in Potential Flow

The criterion for determining which two jump conditions should be used as wake boundary conditions in potential flow is the following. The solution of the resulting boundary value problem should yield flow quantities on configuration surfaces which are relatively insensitive to the assumed wake position as long as that position is not seriously in error. Historically, Eqs. (22) and (23) have been found to satisfy this criterion. Equation (21) is used to determine the wake surface location. An interpretation of this choice is that the potential flow boundary value problem should conserve mass [Eq. (15)] and normal momentum [Eq. (18)], and updating the wake position should lead to conservation of tangential momentum [Eq. (19)] and energy [(Eq. (20)]. In this regard note that the first term on the left of Eq. (18) is negligible when the wake is approximately a stream surface. Once the solution V, p, and ρ to the potential flow boundary value problem is obtained, Eq. (21) becomes an equation for $\hat{n}$, and the wake can be repositioned by a marching procedure. However, a repositioning update is usually unnecessary for any reasonable choice of wake location.

This insensitivity seems to be the case only when the jump in r_P across the wake is small. It is fairly easy to see why. First, assume that the total temperature jump has been scaled out of the problem as discussed in Sec. II.B., so that $r_T = 1$. Since the static pressures are the same on each side of the wake, Eqs. (28–30) show that the magnitude of the mass flux on the side of the wake with higher r_P is greater than that on the other side. As the difference in r_P increases, Eq. (22) tends to a solid wall boundary condition for the side of the wake with higher r_P, and hence, the solution is heavily dependent on wake location. Apparently, the plume and its exterior have become unbalanced and a scaling is required before one can apply Eq. (22).

To find an appropriate scaling, consider Fig. 1. Here, a portion of a wake or slip surface that separates an upper region of total temperature ratio r_T^U and total pressure ratio r_P^U from a lower region with total temperature ratio r_T^L and total pressure ratio r_P^L is shown. Also shown is the estimated or approximate wake location. (For simplicity a two-dimensional case is considered, but these arguments will easily generalize to three dimensions by considering the x direction to be the local stream direction.) Boundary conditions to impose on the approximate wake will be derived by extrapolating upper and lower flux vectors from the real wake to the approximate wake and observing what each conservation law implies about their jump. Let B be a conserved flux vector, e.g., W, a

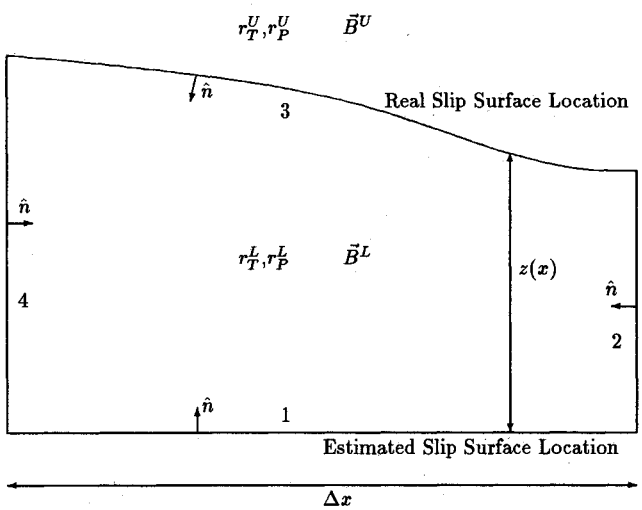

Fig. 1 Schematic diagram for deriving scaling to balance plume flows.

component of $\mathcal{M}$ or $\boldsymbol{E}$. In Fig. 1, only $\boldsymbol{B}^U$ needs to be extrapolated and it is assumed to be divergence-free in the region between the two wake locations (but with $r_T = r_T^U$ and $r_P = r_P^U$). From Gauss's theorem

$$\oint_{1+2+3+4} \hat{\boldsymbol{n}} \cdot \boldsymbol{B}^U \, dS = 0 \tag{38}$$

$$\oint_{1+2+3+4} \hat{\boldsymbol{n}} \cdot \boldsymbol{B}^L \, dS = 0 \tag{39}$$

Multiplying Eq. (38) by the constant λ^U and Eq. (39) by the constant λ^L, subtracting and scaling by Δx leads to

$$\frac{1}{\Delta x}\int_1 \Delta[\lambda \hat{\boldsymbol{z}} \cdot \boldsymbol{B}] \, dS + \frac{1}{\Delta x}\int_{4-2} \Delta[\lambda \hat{\boldsymbol{x}} \cdot \boldsymbol{B}] \, dS + \frac{1}{\Delta x}\int_3 \Delta[\lambda \hat{\boldsymbol{n}} \cdot \boldsymbol{B}] \, dS = 0 \tag{40}$$

Here, Δ denotes the difference between upper and lower values.

First consider conservation of mass and take $\boldsymbol{B}$ to be the mass flux vector $\boldsymbol{W}$. Then, the third integral on the left vanishes identically because the real wake is a stream surface. If λ^U and λ^L are chosen to make the second integral vanish as well, the first integral will yield a jump condition across the approximate wake location satisfied by the real flow. The second integral is an approximation to the expression

$$-\frac{d}{dx}\{z(x)\Delta[\lambda \hat{\boldsymbol{x}} \cdot \boldsymbol{W}]\}|_{z=0} \tag{41}$$

The estimated wake location and slope are assumed to be reasonably close to the real wake location and slope, in which case $z(x)$ and $dz(x)/dx$ are small, and therefore, $\hat{\boldsymbol{x}} \cdot \boldsymbol{W} \simeq pq$. If λ^U was chosen as $\rho^L q^L/\rho^U q^U$ and λ^L as 1, then the expression (41) would vanish identically. However λ^U must be constant. If r_T^U and r_P^U are equal to r_T^L and r_P^L, respectively, then density and speed are continuous across the real wake and λ^U will be nearly equal to 1. If the ratios are unequal then λ^U will still be somewhat invariant, but different than 1. A good choice for λ^U is the far-field value of the above ratio. A reference speed q_r is defined in each region to be the speed at which $p = p_\infty$ in Eq. (28). ρ_r is defined by substituting q_r into Eq. (29), and then choosing $\lambda^U = \rho_r^L q_r^L/\rho_r^U q_r^U$. With this choice, expression (41) is small regardless of moderate errors in wake position and the integrand of the first integral of Eq. (40) becomes the appropriate jump condition. Thus, Eq. (22) is replaced by

$$\Delta[\hat{\boldsymbol{n}} \cdot (\boldsymbol{W}/\rho_r q_r)] = 0 \tag{42}$$

Now, consider conservation of normal momentum and take $\boldsymbol{B}$ to be the z momentum flux, i.e., $\boldsymbol{B} = \boldsymbol{W}(\hat{\boldsymbol{z}} \cdot \boldsymbol{V}) + p\hat{\boldsymbol{z}}$. The third integral of Eq. (40) becomes

$$\frac{1}{\Delta x}\int_3 \hat{\boldsymbol{n}} \cdot \hat{\boldsymbol{z}} \Delta(\lambda p) \, dS \tag{43}$$

again noting that the real wake is a stream surface. Because $\Delta p = 0$ across the real wake, expression (43) vanishes only when $\lambda_U = \lambda_L$. Making this choice, Eq. (40) becomes

$$\frac{\lambda^U}{\Delta x}\int_1 \Delta[(\hat{\boldsymbol{z}} \cdot \boldsymbol{W})(\hat{\boldsymbol{z}} \cdot \boldsymbol{V})] + \Delta p \, dS + \frac{\lambda^U}{\Delta x}\int_{4-2} \Delta[(\hat{\boldsymbol{x}} \cdot \boldsymbol{W})(\hat{\boldsymbol{z}} \cdot \boldsymbol{V})] \, dS = 0 \tag{44}$$

The second integral approximates

$$-\lambda^U \frac{d}{dx}\{z(x)\Delta[(\hat{\boldsymbol{x}} \cdot \boldsymbol{W})(\hat{\boldsymbol{z}} \cdot \boldsymbol{V})]\} \tag{45}$$

Again assuming that the approximate wake position and slope are reasonably close to the real wake position and slope, then $z(x)$, $dz(x)/dx$, and $\hat{\boldsymbol{z}} \cdot \boldsymbol{V}$ are all small, so that this integral may be neglected. In the first integral of Eq. (44) both $\hat{\boldsymbol{z}} \cdot \boldsymbol{W}$ and $\hat{\boldsymbol{z}} \cdot \boldsymbol{V}$ are small so that their product is negligible. Thus, the boundary condition implying conservation of normal momentum is still Eq. (23).

In a similar manner, consideration of conservation of tangential momentum and energy leads to the conclusion that the wake updating condition should be

$$\alpha[\hat{\boldsymbol{n}} \cdot (\boldsymbol{W}/\rho_r q_r)] = 0 \tag{46}$$

The consequences of the analysis of this section are somewhat clearer if the wake boundary conditions are interpreted in terms of a scaling. In each separate region of constant total temperature and pressure ratios, scaled (or starred) velocity, density, and pressure are defined as follows:

$$\begin{aligned} \boldsymbol{V}^* &= (1/Q)\boldsymbol{V} \\ \rho^* &= (1/R)\rho \\ p^* &= (1/RQ^2)p \end{aligned} \tag{47}$$

Here Q and R are constants associated with the region. A consistent set of associated scaled quantities are the following:

$$\begin{gathered} \Phi^* = (1/Q)\Phi, \quad q^* = (1/Q)q, \quad c^* = (1/Q)c \\ M^* = M, \quad H^* = (1/Q^2)H, \quad S^* = S \\ \boldsymbol{W}^* = (1/RQ)\boldsymbol{W}, \quad r_T^* = (1/Q^2)r_T, \quad r_P^* = (1/RQ^2)r_P \end{gathered} \tag{48}$$

In order to achieve Eq. (42) as a natural boundary condition for the scaled mass flux vector, $QR = q_r\rho_r/q_\infty\rho_\infty$ is required. For the purpose of simulating wakes in the far field by doublet sheets which are constant in the freestream direction, $q^* \to q_\infty$ as $p^* \to p_\infty$ is required. These two requirements imply

$$\begin{aligned} Q &= (q_r/q_\infty) \\ &= \sqrt{r_T}\sqrt{1 + \{2/[(\gamma - 1)]M_\infty^2\}(1 - r_P^{-(\gamma-1)/\gamma})} \\ R &= (\rho_r/\rho_\infty) = [r_P^{(\gamma-1)/\gamma} r_T] \end{aligned} \tag{49}$$

Note that when $r_P = 1$, this scaling reduces to that of Sec. II.B. Moreover, for arbitrary values of r_P, the relationships between scaled and unscaled Mach numbers, pressures, momenta, and streamlines are independent of r_T. For the scaled quantities equations, Eqs. (1), (22), and (36) hold as before, and Eq. (21) is used to update the wake. However, Eq. (23) no longer holds for p^*. Nevertheless, this scaling does imply that both ρ^* and $\hat{n}\cdot V^*$ are continuous across wakes, a well-known property of the unscaled equivalents in the case when there is no jump in total temperature and pressure ratios across the wake.

E. Implementation of the Static Pressure Boundary Condition

Most full potential solvers can handle a Neumann jump condition of the form

$$\Delta(W^*\cdot\hat{n}) = 0 \tag{50}$$

or a Dirichlet jump condition of the form

$$\Delta(\Phi^*) = \mu^* \tag{51}$$

The static pressure boundary condition [Eq. (23)] is not a Dirichlet condition, but is somewhat related. From Eqs. (23) and (28), $Q^2R(q_\infty^2 - q^{*2})$ is found to be continuous across wakes. Upon some manipulation, this implies that

$$\alpha(V^*)\cdot\Delta(V^*) = [\Delta(Q^2R)\alpha(q_\infty^2 - q^{*2})]/[2\alpha(Q^2R)] \tag{52}$$

Substituting Eq. (51) into the left side of Eq. (52) and using the fact that $\hat{n}\cdot V^*$ is continuous across wakes, gives

$$\alpha(V^*)\cdot\nabla\mu^* = [\Delta(Q^2R)\alpha(q_\infty^2 - q^{*2})]/[2\alpha(Q^2R)] \tag{53}$$

Now Q^2R is a function of r_P only. Usually, the dependence is fairly weak. If it is assumed that $\Delta(Q^2R)/\alpha(Q^2R)$ is small, then Eq. (53) can be interpreted as a convection equation for μ^*. Also, assuming an estimate of V^* from a previous iteration, Eq. (53) can be integrated along corresponding wake surface streamlines. For this purpose a Kutta condition must be applied along the wake leading edge to determine the initial value of μ^* along each streamline. Once μ^* is obtained everywhere on the wake surface, Eqs. (50) and (51) become the standard wake jump conditions for a full-potential solver.

III. TRANAIR Formulation and Discretization

In TRANAIR[1] the boundary surfaces of objects to be modeled are described using networks of piecewise flat surface patches called panels, with curvature simulated by linearly varying normals. This input format allows relatively simple specification of complicated surfaces. A finite element solution is obtained on a sequence of volume grids that are generated automatically. Underlying the grid is a uniform rectangular grid, called the global grid, that contains all the boundary surfaces but is otherwise independent of them. This global grid is used to enforce the far-field condition as well as to apply the Prandtl-Glauert preconditioner.[1] The global grid is refined locally in a hierarchical manner, i.e, any grid box can be refined into eight geometrically similar boxes (four in two dimensions). This process is repeated to give a grid with any desired local resolution. This process is controlled in various ways, one of which is a solution adaptive procedure.[2] The degree of resolution required is determined by a local error estimation procedure on each of a sequence of intermediate grids.

The nonlinear boundary-value problem is discretized on each grid using a finite element method. The discrete unknowns are the values of ϕ defined at the grid points, i.e., corners of grid boxes. The velocity is computed at centroids of the finite elements and used to compute a density. In the nonlinear case, the density is treated as constant in each region so that it can be factored out of the element stiffness matrix. Elements cut by boundaries have special element stiffness matrices as well as special formulas for computing velocities at centroids of regions. The finite element integrals are computed on the portion of the grid box cut off by the boundary surface.

In regions of supercritical flow, artificial dissipation must be introduced to rule out expansion shocks. Upwinding the density using adjacent element values produces a first-order upwinding where ρ is replaced by $\tilde{\rho}$, defined by

$$\tilde{\rho} = \rho - \nu_1\hat{V}\cdot\boldsymbol{D}_-\rho \tag{54}$$

where $\hat{V}$ is the normalized local velocity, $\boldsymbol{D}_-\rho$ is an upwind undivided difference, and here ν_1 is a switching function used to turn on upwinding in supersonic zones. It has been observed that more grid resolution seems to be required in supersonic zones by this method than in subsonic zones. This observation has led to the implementation of a second-order upwinding where ρ is replaced by $\tilde{\tilde{\rho}}$, defined by

$$\tilde{\tilde{\rho}} = \tilde{\rho} + \nu_2\hat{V}\cdot\boldsymbol{D}_-\tilde{\rho} \tag{55}$$

When modeling powered plumes, it was shown in Sec. II that the choice of Eqs. (23) and (42) gives a full potential solution that is relatively insensitive to small changes in the wake position. Equation (46) is enforced by allowing the wake position to change. In principle, it is possible to solve this complete nonlinear system.[6] However, difficulties arise in keeping the resulting wake surfaces coherent and with regard to convergence. In TRANAIR, a feature is available that lofts the wake surface in the normal direction at the end of a run. The amount of movement is proportional to the local value of $\hat{n}\cdot\alpha W^*$.

In TRANAIR the wake surface is paneled and discretized with values of μ^* defined at panel corner points. Values of μ^* and its gradient at any location on the wake are computed using a suitable interpolation procedure. Equation (53) holds at panel edge midpoints using values of V^* calculated from the local basis functions for Φ^*. This arrangement assumes that the local flow direction is roughly parallel to panel columns. If there is substantial crossflow, implementation of Eq. (53) can lead to difficulties and therefore is replaced by

$$\alpha(q^*)\hat{V}_\infty\cdot\nabla\mu^* = [\Delta(Q^2R)\alpha(q_\infty^2 - q^{*2})]/[2\alpha(Q^2R)] \tag{56}$$

Such direction limiting is overly severe and is currently being investigated.

At each leading-edge panel corner point of a wake a Kutta condition is applied. This condition takes the form

$$\mu^* - \Delta(\Phi^*) + \varepsilon\hat{t}\cdot\nabla[\mu^* - \Delta\Phi^*] = 0 \tag{57}$$

Here $\hat{t}$ is a unit tangent vector lying along the corresponding panel column edge, and ε is a small parameter which is chosen to be approximately equal to the local field mesh size in the $\hat{t}$ direction. This equation guarantees that μ^* is the jump in the basis function potential Φ^* in the case where wake panels are denser than the field grid. The derivative term is added to take care of the possibility that the previous condition is redundant with respect to the boundary condition Eq. (51). In this case, Eq. (57) ensures that the jump in basis function velocity is well-defined and finite.

The nonlinear equations for ϕ and μ^* are solved using a preconditioned inexact Newton method.[1] The TRANAIR formulation described here has been implemented for problems in both two- and three-space dimensions. An option in the two-dimensional code allows the calculation of axisymmetric flows.

IV. Euler Formulation

For this article, the solution to the Euler equations is calculated numerically using the PARC2D computer program,[3] which is based on another program, ARC2D.[7] A body-fitted, structured grid is used to discretize the flowfield. The discretization of the Euler equations is conservative and second-order accurate. Artificial dissipation is added to ensure a stable algorithm and to prevent overshoots at shock waves. The artificial dissipation is a combination of second-order and fourth-order differences.[8] The effect of the second-order dissipation is to spread a discontinuity into a smooth wave spanning four or five grid points. As the grid spacing is reduced this smooth wave approaches the discontinuous solution to the Euler equations. So the spatial discretization used by PARC2D is consistent—the numerical solution approaches the exact solution as the grid spacing is reduced. PARC2D uses an approximate factorization iterative, implicit algorithm to find the solution to the steady Euler equations.[9]

Four types of boundary conditions are used by PARC for problems solved in this article. For grid points on solid surfaces the velocity is specified to be tangent to the surface, while the pressure, density, and Mach number are extrapolated from the nearest interior point. On the upstream boundaries a subsonic inflow boundary condition is used. The total pressure and total temperature are specified, and the velocity is set to be normal to the grid line on which the boundary condition is set. For the problems solved in this article the inflow velocity is axial, i.e., it has no radial component. Also, the total pressure and total temperature are specified to be constant on the inflow boundary within each stream, although different values are used for each of the three upstream boundaries. The subsonic inflow boundary condition treatment is completed by extrapolating from the nearest interior point the characteristic-like quantity

$$u_N - P/(\rho c) \tag{58}$$

where u_N is the velocity normal to the grid line and P is the static pressure.

At the outflow boundary, 20 nacelle radii downstream of the trailing edge of the plug, the type of boundary condition applied depends on the Mach number of the nearest interior point. If this Mach number is greater than 1.0, all flow quantities on the boundary point are extrapolated from the interior point. If the Mach number is less than 1.0, the static pressure on the boundary point is specified, while the density and two velocity components are extrapolated from the interior point. The outermost grid line is a line of constant radius, 17 nacelle radii from the axis. The solid wall boundary condition is applied along this grid line. The axis of symmetry is excluded from the domain by extending the plug along a line of constant radius which is 0.03 nacelle radii from the axis.

V. Test Cases

The turbofan nozzle chosen as a test case is one for which there is data from a static test designed to validate axisymmetric CFD codes.[10] The use of an axisymmetric test case allows the use of extremely dense computational grids, even though both computer codes used here are capable of fully three-dimensional calculations.

For the PARC runs, the model was truncated upstream as shown in Fig. 2a and an upstream boundary condition was applied. The geometry used for the TRANAIR runs is shown in Fig. 2b.

Given the geometry of the nozzle, five parameters are needed to specify the boundary conditions for the solution of the Euler equations. These are the external Mach number, the fan pressure ratio, P_{T_F}/p_∞, the primary pressure ratio, P_{T_P}/p_∞, and the ratio of the total temperature in each stream to the exterior static temperature. For the potential flow solution, the location of the wakes must also be specified. As shown in Sec. II, the Mach number and pressure fields are independent of the temperature ratios, so these ratios were chosen to be 1.0 for all computations. The values for the pressure ratios were chosen to match specific conditions from the static nozzle test. A high pressure ratio was chosen to compare the computed predictions of the system of expansions and compressions that occur in these nozzle flows and is typical of conditions at which turbofans operate. Two exterior Mach numbers were chosen: 1) $M_\infty = 0.1$ to simulate the static test and 2) $M_\infty = 0.83$ to reflect the cruise Mach number of a transonic transport. Table 1 summarizes the boundary conditions for the two test cases. Further flow conditions were analyzed and results can be found in Ref. 11.

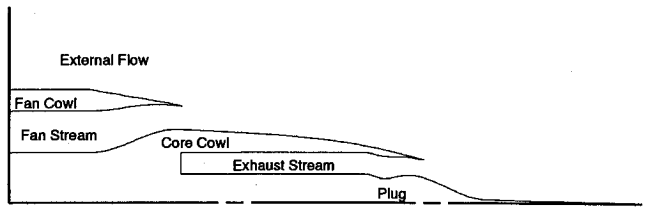

a) PARC geometry

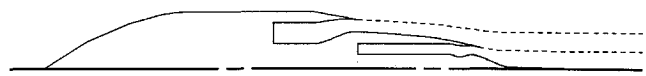

b) TRANAIR geometry

Fig. 2 Geometry used for PARC and TRANAIR.

Table 1 Flow conditions for two test cases

Case	Mach	Fan P_T/p_∞	Exhaust P_T/p_∞
1	0.83	2.808	2.163
2	0.10	2.808	2.163

VI. Computational Results

To control the discretization errors the calculations were performed on a sequence of increasingly finer grids. Tables 2 and 3 summarize the grids used for the two codes. Not all grids were run in both cases. The densest of these grids were only used to check that the solution was essentially grid converged, i.e., that the solution would not change appreciably with further grid refinement. Full details of solutions on the sequences of grids can be found in Ref. 11. For the TRANAIR results, solution adaptive gridding was used, resulting in slight differences in the grids from case to case. However, the adaptive gridding strategy was chosen to obtain essentially uniform grid refinement in the fan stream.

A further source of discretization error in the TRANAIR results occurs if the wakes are not stream surfaces. To reduce this source of error, solutions were first obtained with wakes generated to maintain a constant cross-sectional area in the plumes as shown in Fig. 2. The plume lofting feature in TRANAIR then yielded a new wake position for which the code was run a second time. In both cases, the flow through the wake surface, representing the error in the assumed wake position, was reduced to the level of truncation error in the second run. The results shown here used grids fine enough so that further refinement caused no significant changes in the solution.

A. Case 1 Results

Case 1 reflects commercial transport cruise conditions. Sample grids are shown in Fig. 3 (PARC grid P2) and Fig. 4 (TRANAIR grid T3). Finer grids were too dense to be meaningfully pictured here. For the TRANAIR results with second-order upwinding, grids T1–T5 were used, for first-order

Table 2 TRANAIR grids used for axisymmetric calculations

Grid	Fan stream grid (approx.) (axial × radial)	Total grid cells
T1	50 × 5	2,000
T2	100 × 10	5,000
T3	200 × 20	17,000
T4	400 × 40	65,000
T5	800 × 80	270,000
T6	1600 × 160	600,000

Table 3 PARC grids used for axisymmetric calculations

Grid	Fan stream grid (axial × radial)	Total grid cells
P1	64 × 16	7,300
P2	128 × 32	28,400
P3	256 × 64	112,100
P4	512 × 128	223,600

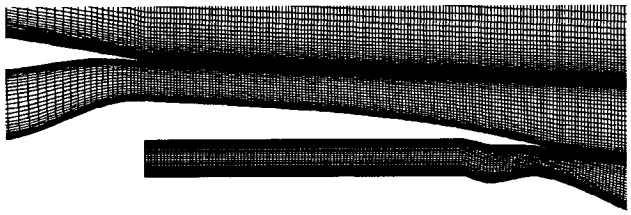

Fig. 3 Medium PARC axisymmetric grid P2, closeup view.

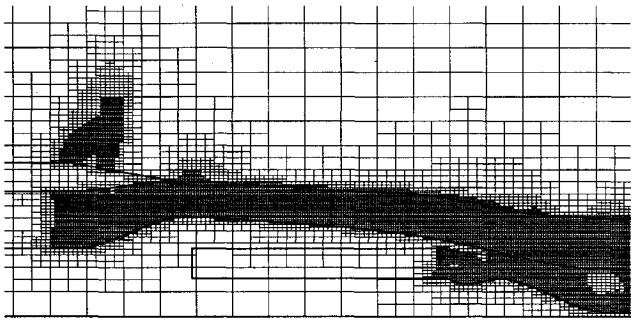

Fig. 4 TRANAIR grid T3 for case 1, closeup view, $M_\infty = 0.83$, fan $P_T/p_\infty = 2.808$.

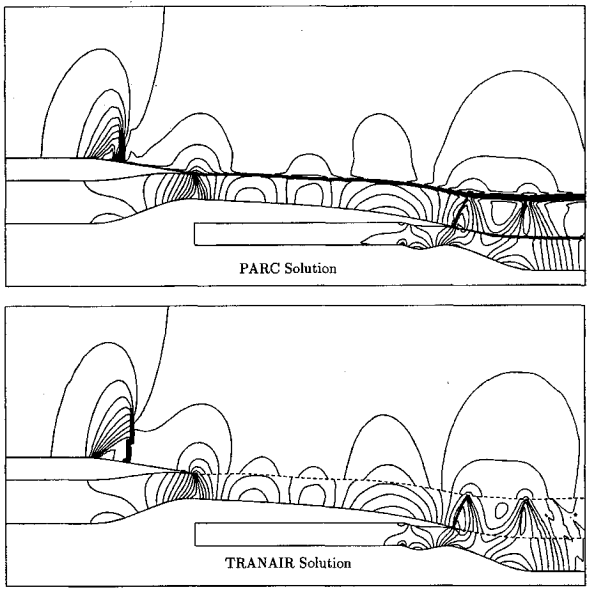

Fig. 5 Mach number contours for PARC solution on grid P3 and TRANAIR solution on grid T5 for case 1, $M_\infty = 0.83$, fan $P_T/p_\infty = 2.808$.

upwinding, grid T6 was also used. Grids T5 and P3 have approximately the same radial grid density. Figure 5 shows contour plots of the Mach number from the PARC solution on the P3 grid and from the TRANAIR solution using second-order upwinding on the T5 grid. The contours are at a spacing of $\Delta M = 0.05$. These contour plots show good agreement.

Figure 6 compares static pressures on the core cowl. In the configuration geometry shown in Fig. 6 the core cowl is shown with a dashed line. The solutions shown are the TRANAIR solution on the T6 grid with first-order upwinding, the TRANAIR solution on the T5 grid with second-order upwinding, and the PARC solution on the P3 grid.

In order to show the effect of wake position on the TRANAIR results, the lofted and unlofted wake positions and the resulting static pressures on the core cowl using second-order upwinding on grid T5 are compared in Fig. 7.

B. Case 2 Results

In case 2 the low freestream Mach number of 0.1 eliminates the suppression of the nozzle evident in case 1. This means that the pressure at the exit of the fan nozzle is lower, resulting in a larger number of compression and expansion waves. Figure 8 shows contour plots of the Mach number on the P4 PARC grid and the T4 TRANAIR grid using second-order upwinding. Again, the contours are at a spacing of $\Delta M = 0.05$. The agreement is quite good.

Figure 9 compares computed static pressures on the core cowl. The solutions shown are the TRANAIR solution on the T4 grid with second-order upwinding, the TRANAIR solution

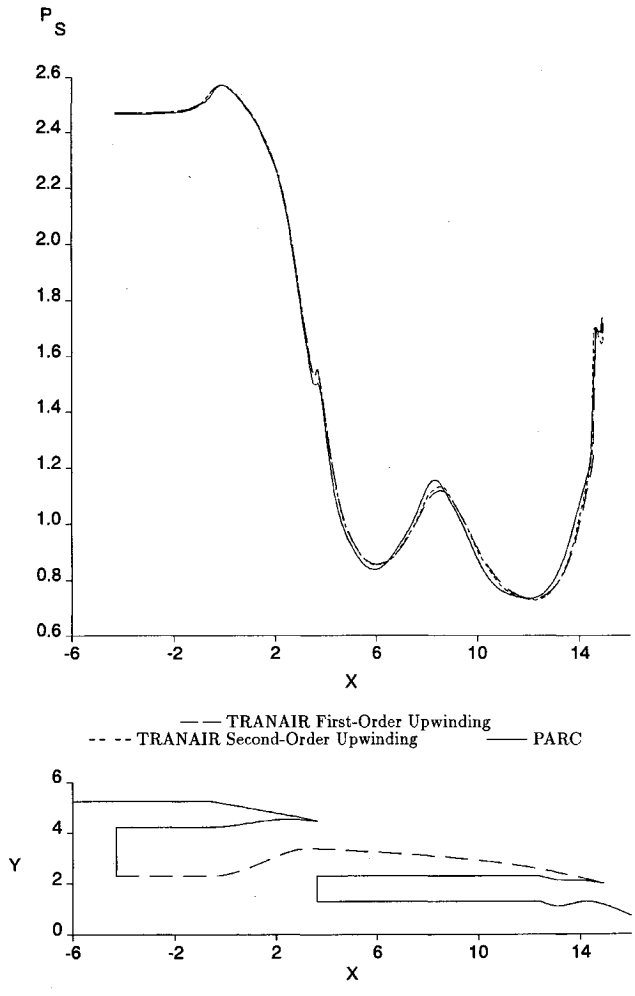

Fig. 6 Static pressure on the core cowl. PARC vs TRANAIR with first-order upwinding vs TRANAIR with second-order upwinding for case 1, $M_\infty = 0.83$, fan $P_T/p_\infty = 2.808$.

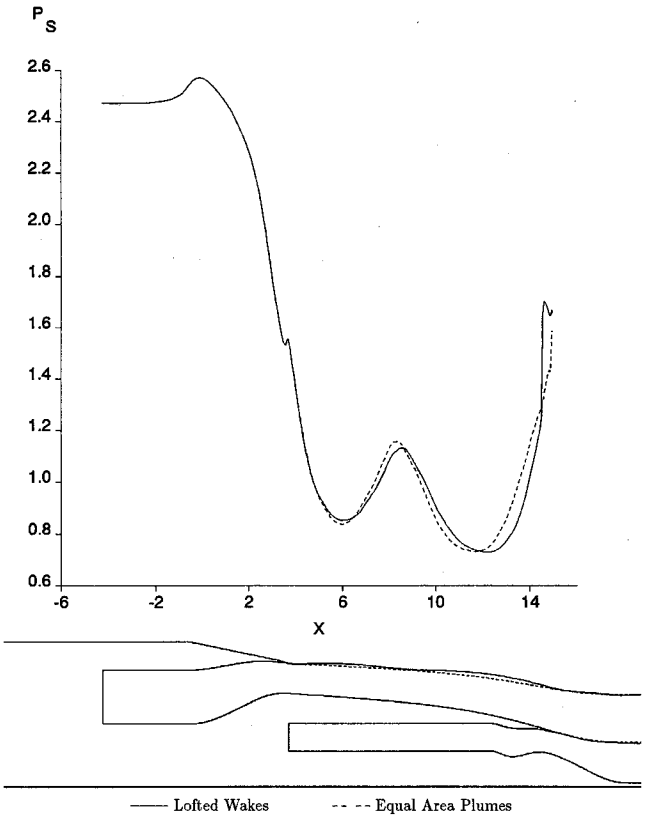

Fig. 7 Static pressure on the core cowl. TRANAIR with equal area plumes and lofted wakes with second-order upwinding on grid T5 for case 1, $M_\infty = 0.83$, and fan $P_T/p_\infty = 2.808$.

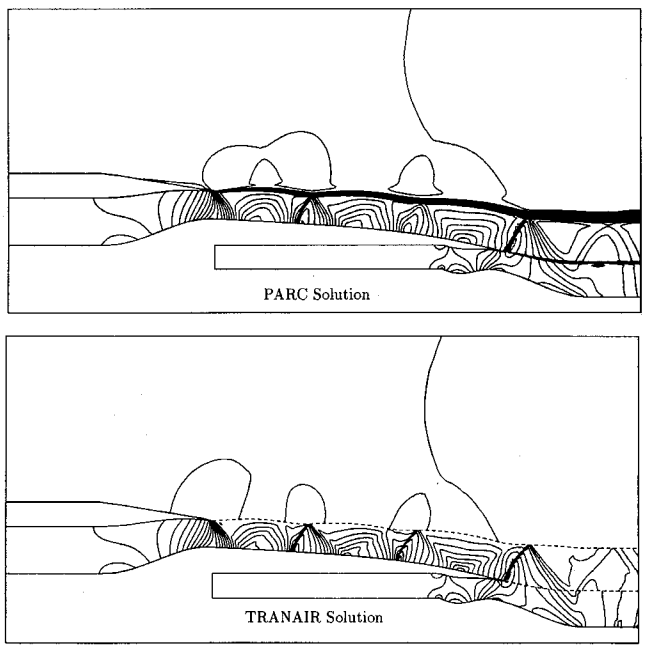

Fig. 8 Mach number contours for P4 grid PARC solution and for T4 grid TRANAIR solution using second-order upwinding for case 2, $M_\infty = 0.1$, fan $P_T/p_\infty = 2.808$.

on the T6 grid using first-order upwinding, and the PARC solution on the P4 grid. The static test data[10] are also shown. The PARC solution evidently falls between the TRANAIR first- and second-order upwinding results. The code results are in close agreement, but the codes and test data show differences in the amplitudes of pressure peaks and valleys and a phase shift. Viscous effects are probably significant in this case. Results reported elsewhere[12] indicate that viscous

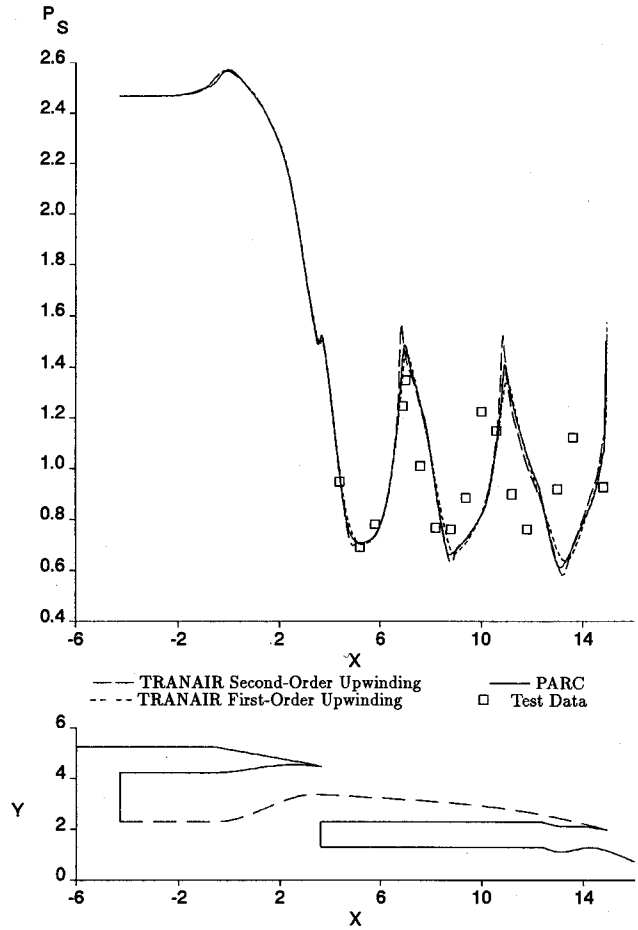

Fig. 9 Static pressure on the core cowl. PARC vs TRANAIR with first-order upwinding vs TRANAIR with second-order upwinding for case 2, $M_\infty = 0.1$, fan $P_T/p_\infty = 2.808$.

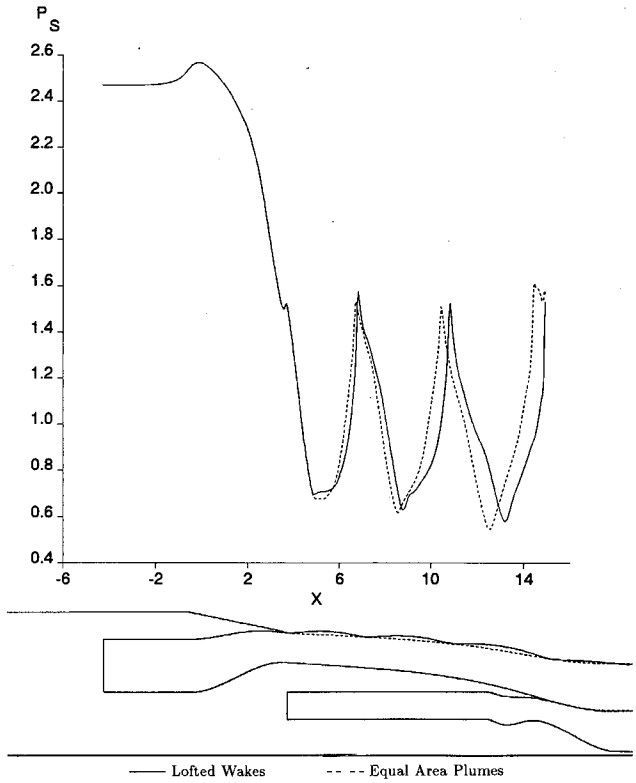

Fig. 10 Static pressure on the core cowl. TRANAIR with equal area plumes and lofted wakes using second-order upwinding on the T4 grid for case 2, $M_\infty = 0.1$, and fan $P_T/p_\infty = 2.808$.

effects provide a mechanism capable of causing these differences and it is expected that the inclusion of viscous effects will reduce the discrepancies. Further studies are underway that include viscous modeling which in the case of TRANAIR involves solution of boundary-layer and shear-layer equations. A note of caution must be added though, as for some cases the solution in a supersonic jet plume can be very sensitive to the choice of turbulence model. Another factor may be the 1% variation in total pressure across the fan stream in the test.

As for case 1, the TRANAIR solutions were obtained with wakes generated to maintain a constant cross-sectional area in the plumes and with lofted plumes. The wake positions and the resulting static pressures on the core cowl are compared in Fig. 10. The shift in position of the waves is more noticeable than in case 1.

VII. Conclusions

Two formulations and codes for modeling engine exhausts have been compared. For some problems of interest, it has been shown that an appropriate full potential model can provide results that are quite close to those obtained with Euler equations modeling. Further investigation of the differences between the code results and the static test data needs to be undertaken.

References

[1]Young, D. P., Melvin, R. G., Bieterman, M. B., Johnson, F. T., Samant, S. S., and Bussoletti, J. E., "A Locally Refined Rectangular Grid Finite Element Method: Application to Computational Fluid Dynamics and Computational Physics," *Journal of Computational Physics*, Vol. 92, No. 1, 1991, pp. 1–66.

[2]Bieterman, M. B., Bussoletti, J. E., Hilmes, C. L., Johnson, F. T., Melvin, R. G., Samant, S. S., and Young, D. P., "Solution Adaptive Local Rectangular Grid Refinement for Transonic Aerodynamic Flow Problems," *Proceedings of the Eighth GAMM Conference on Numerical Methods in Fluid Mechanics*, edited by P. Wesseling, Vieweg Verlag, Braunschweig, 1990, pp. 22–31.

[3]Cooper, G. K., "The PARC Code: Theory and Usage," Arnold Engineering Development Center Technical Rept. 87-24, 1987.

[4]Munk, M., and Prim, R.,"On the Multiplicity of Steady Gas Flows Having the Same Streamline Pattern," *Proceedings of the National Academy of Sciences*, Vol. 33, 1947, pp. 137–141.

[5]Serrin, J., "Mathematical Principles of Classical Fluid Mechanics," *Handbuch der Physik*, Springer-Verlag, Berlin, 1960, pp. 125–263.

[6]Tinoco, E. N., Lu, P., and Johnson, F. T., "An Improved Panel Method for the Solution of Three-Dimensional Leading-Edge Vortex Flows," NASA CR-3279, July 1980.

[7]Pulliam, T. H., and Steger, J. L., "Implicit Finite-Difference Simulations of Three Dimensional Compressible Flow," *AIAA Journal*, Vol. 18, No. 2, 1980, pp. 159–167.

[8]Jameson A., Schmidt, W., and Turkel, E., "Numerical Solutions of the Euler Equations by Finite Volume Methods Using Runge-Kutta Time-Stepping Schemes," AIAA Paper 81-1259, 1981.

[9]Beam, R., and Warming, R. F., "An Implicit Finite-Difference Algorithm for Hyperbolic Systems in Conservation-Law Form," *Journal of Computational Physics*, Vol. 22, No. 1, 1976, pp. 87–110.

[10]Brown, J. J., "Axisymmetric Nozzle Database," Boeing Document D6-52891, Seattle, WA, March 1985.

[11]Johnson, F. T., Melvin, R. G., Young, D. P., Foutch, D. W., Bussoletti, J. E., and Bieterman, M. B., "Propulsion System Exhaust Simulation Using Full Potential and Euler Formulations," Boeing Document D6-55792TN, Seattle, WA, April 1991.

[12]Keith, B. D., Uenishi, K., and Dietrich, D. A., "CFD-Based Three-Dimensional Turbofan Exhaust Nozzle Analysis System," AIAA Paper 91-2478, June 1991.